Conjugate heat transfer analysis of the transient thermal discharge of a metallic latent heat storage system

Journal of Physics: Conference Series **2766** (2024) 012212 doi:10.1088/1742-6596/2766/1/012212

Conjugate heat transfer analysis of the transient thermal discharge of a metallic latent heat storage system

F Nees and Y S Pai

German Aerospace Center (DLR), Institute of Vehicle Concepts,
Pfaffenwaldring 38-40, 70569 Stuttgart, Germany

E-Mail: frank.nees@dlr.de

Abstract. Thermal energy storage systems utilizing metallic phase change materials exhibit great potential as a technology for mobile applications, offering high storage densities and high thermal discharge rates. First experimental investigations show the functionality and performance characteristics of this system. For a deeper understanding of the thermal discharge, this paper presents a numerical model and analysis of the transient conjugate heat transfer. For validation of the numerical model, the results of the simulations are compared to the available experimental data. The investigated storage is based on an aluminum silicon alloy and a box-shaped graphite container design. In this system, heat extraction is achieved by forced convection of ambient air. The transient thermal discharge was simulated from 650 °C to 100 °C, and the solidification of the storage material at around 577 °C was simulated using an enthalpy-porosity approach. The discharge time and total heat flow show good agreement with the experimental data, indicating the model's successful validation. An empirical study was carried out to determine the thermal contact resistance at the interface between the storage material and the graphite container. The present study contributes new physical insights regarding the thermal discharge of a novel metallic latent heat thermal energy storage system.

1. Introduction

Innovative heat storage systems have the potential to enable new thermal management concepts for battery electric vehicles. In the cold season, the energy consumption for cabin heating and preheating of vehicle components can exceed the energy demand for traction and is therefore a challenging issue [1,2]. Compared to today's battery powered electric heaters or heat pumps, the electrical energy requirement can be reduced by thermal energy storages, resulting in significant improvements in the effective range, especially for battery electric buses. One of the most promising storage technologies for mobile applications are metallic latent heat thermal energy storage systems (LHTES). Metallic phase change materials (mPCMs) offer high storage densities and high thermal conductivities, allowing for fast charging and discharging [3-5]. During charging, heat is generated by electric heaters and stored in the storage material in the form of sensible and latent heat. The stored heat is then utilized during discharging to regulate the temperature of the cabin or components, thereby conserving battery capacity. Kraft et al. [6] and Luo et al. [7] showed already the principal concept and potential of such a storage system for a vehicle application.

However, there is a need for a better understanding of the physics and thermal behavior involved, in particular for the heat extraction process. First extensive experimental measurements of the thermal discharge characteristics of a lab-scale prototype configuration using mPCM as storage material was performed by Nees et al., thus showing the functionality and performance [8,9]. For a deeper analysis

of the transient discharge, this paper presents a three-dimensional computational fluid dynamics (CFD) model of the previous experimentally investigated prototype for the first time. For validation of the numerical model, the results of the simulations are compared to available experimental data. In order to elucidate the transitional character of the discharge, the conjugate model considers the phase change of the storage material, the air flow in the fluid channels and the intermediate solid layers including an analysis of the thermal contact resistances. The resulting temperature distribution and heat flow are analyzed in the temperature range from 650 °C to 100 °C.

2. Model description

The conjugate heat transfer analysis (CHT) is modelled and simulated using the commercial software ANSYS FLUENT, Version 2021 R2. The geometry and boundary conditions of the model are chosen carefully in order to fit the real conditions of the experimental investigation and to enable a validation of the model later on. Nevertheless, useful simplifications and assumptions are defined to simplify the model where possible to save calculation time and numerical resources.

Figure 1 shows the schematic representation of the prototype design and experimental setup. More details about the prototype and the experimental investigation are reported elsewhere [9]. The storage is based on the aluminum silicon alloy $AlSi_{12}$ and a box-shaped graphite container design. The container is pressurized with argon and confined by a steel container. An installed steel plate on the bottom side contains electric heaters for charging and fluid channels for discharging.

In the experiment, the heat extraction was achieved by forced convection of ambient air utilizing a controllable fan. The air channel geometry consists of parallel rectangular channels. In table 1, relevant geometrical details of the prototype and the fluid channel geometry for heat extraction are listed.

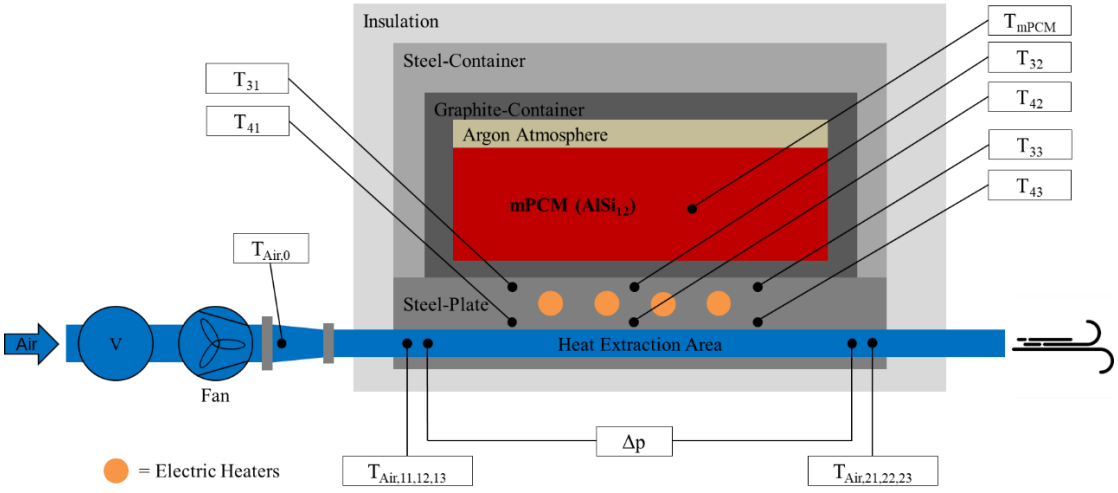

Figure 1. Schematic representation of the prototype design and experimental setup [9].

Table 1. Geometrical details of the prototype and air channels.

Item	Specification
Total dimension (with insulation)	0.33 x 0.33 x 0.15 m (L x W x H)
Base area fluid channels and $AlSi_{12}$	0.18 x 0.18 m (L x W)
Air channel geometry	10 x 4.85 mm (H x W), 28 parallel rectangular channels
Air channel hydraulic diameter	6.53 mm
Fin thickness	1.65 mm

For the numerical model, the geometry is simplified by modelling only one fluid channel, respectively two half channels, instead of modelling 28 multiple channels of the real geometry.

Therefore, the symmetrical structure of the geometry is exploited by applying symmetry boundaries with the assumption of equal fluid mass flow through each channel in the prototype.

The electric heaters as well as other inconsequential components such as screws are not modelled to simplify the geometry. The insulation around the mPCM casings is also not simulated and an adiabatic boundary is assumed in the domain. Heat losses to the environment are neglected. Figure 2 shows the three-dimensional numerical model with selected boundary conditions.

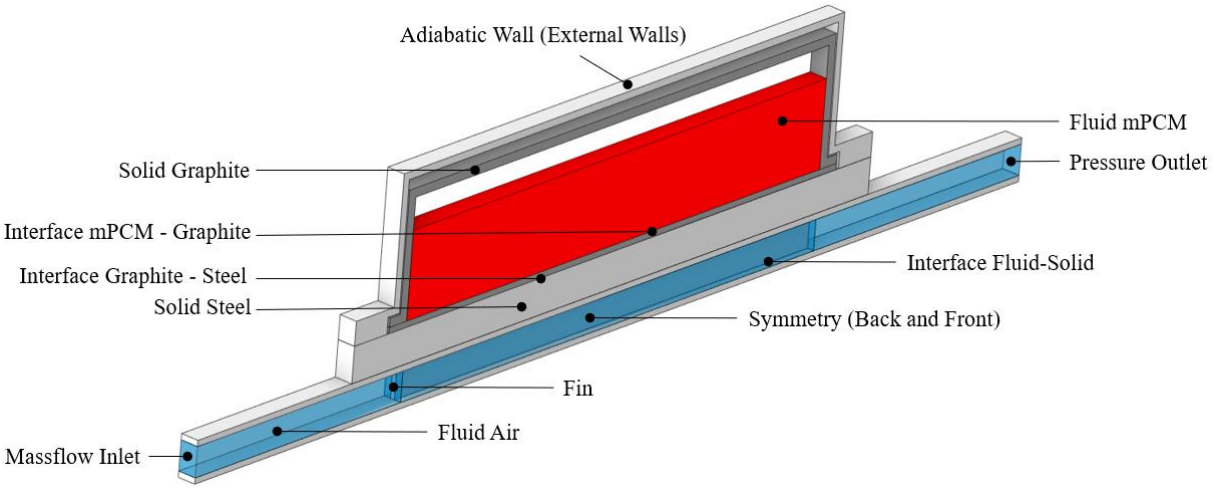

Figure 2. Three-dimensional numerical model with selected boundary conditions.

The solid material properties such as thermal conductivity and specific heat capacity are defined as a function of temperature. The fluid properties such as density, thermal conductivity, specific heat capacity, dynamic viscosity and kinematic viscosity are temperature dependent. For the transient simulation, only the temperature field is fully transient, whereas the transient phenomena in the flow field are not modelled. The fluid flow problem in this case, is similar to a steady-state model with the temperature boundary condition varying over time. Therefore, a sufficiently large time step could be selected. In this study, a time step of 10 s was chosen.

In order to have an appropriate mesh size for an accurate numerical solution, a Richardson extrapolation was performed as grid convergence study, which shows that the chosen mesh is sufficient and there is no need for further refinement. Hexahedral meshes were used, with inflation prism layers at the air fluid-solid interface to refine the near wall boundary region.

At the inlet of the numerical domain, a constant air mass flow of 0.54 kg/h was set for the whole discharge time, which corresponds to a total mass flow of 15 kg/h in the experiments. The dedicated Reynolds number in the rectangular fluid channel varies between 530 and 1072, depending on the air bulk temperature. As the Reynolds number is much smaller than 2300, the laminar flow model is selected for the air flow solution. The initial temperature conditions for fluid and solid regions are selected based on experimental data, with an initial mPCM temperature of 650 °C. The air temperature at the inlet boundary is selected based on experimental data and drops with a progress in discharge time. Thermal radiation inside the fluid channel is modelled using the surface to surface radiation model. At the air fluid-solid interfaces, a thermally coupled wall boundary condition is defined.

For the numerical modelling of the phase change, the enthalpy-porosity model in the solidification and melting model of ANSYS FLUENT is selected. The energy equation for the phase change can be written as follows:

$$\frac{\partial}{\partial t}(\rho H) + \nabla \cdot (\rho \vec{v} H) = \nabla \cdot (k \nabla T) + S \tag{1}$$

where H is the enthalpy, ρ the density, $\vec{v}$ the fluid velocity, k the thermal conductivity and S the source term. The liquidus and solidus temperatures are defined as 579 °C and 575 °C, respectively. For the

phase change of the mPCM, gravitational effects and natural convection flow within the mPCM volume are neglected, since the heat discharge is realized on the bottom side. Thus, the heat conduction is the predominant mode of heat transfer within the mPCM volume. Moreover, volumetric changes due to phase change are not modelled.

At the contact interface between mPCM and graphite, a temperature dependent contact resistance is defined using a shell conduction layer. The values of the thermal contact resistance are empirically determined with the constraint to fit the discharge time and heat flow and the results are presented in table 2. At the interface between graphite and the heating steel plate, a constant thermal contact resistance of 2.5 cm^2K/W is defined using a thin wall boundary condition.

The resulting heat flow from the simulation is calculated from an energy balance of the air mass flow, the average heat capacity of the air and the temperature difference between the air temperatures at the aligned positions with the thermocouples in the experiment $T_{Air,0}$, $T_{Air,1}$ and $T_{Air,2}$.

3. Results and discussion

For the validation of the numerical model, the simulation results are compared to the experimental data for the same set of parameters such as a total air mass flow of 15 kg/h. Figure 3(a) shows the results of the temperature of the mPCM, heating steel plate T_{HP} and outlet air temperature $T_{Air,2}$ against the discharge time obtained from the simulation with the experimental data. The total time for the thermal discharge of the mPCM from T_{mPCM} of 650 °C to 100 °C, as predicted by the numerical model, differs by about 5% from the experiment. Overall, the temperature curves show strong agreement with the experiment.

Figure 3(b) illustrates the heat flow against the mPCM temperature obtained from the simulation with the experimental data. The heat flow curves are consistent in the temperature range of 650 °C to 100 °C. In the liquid state, the heat flow predicted in the simulation differs by about 1 to 2% from the mean experimental values, except for the initial start-up phase at 650 °C, where the deviations are higher. In the solid state, the deviation from simulation to the mean experimental values is about 2%. This implies that the presented transient heat discharge simulation can be used to examine the heat extraction characteristics with sufficient accuracy and the numerical model can be regarded as validated.

The phase change takes place at a temperature around 577 °C and is visible in figure 3(a) by the plateau of the mPCM temperature against time. In figure 3(b), the transition from liquid to solid is noticeable by the clear drop in heat flow caused by the increased thermal contact resistance at the mPCM-graphite interface.

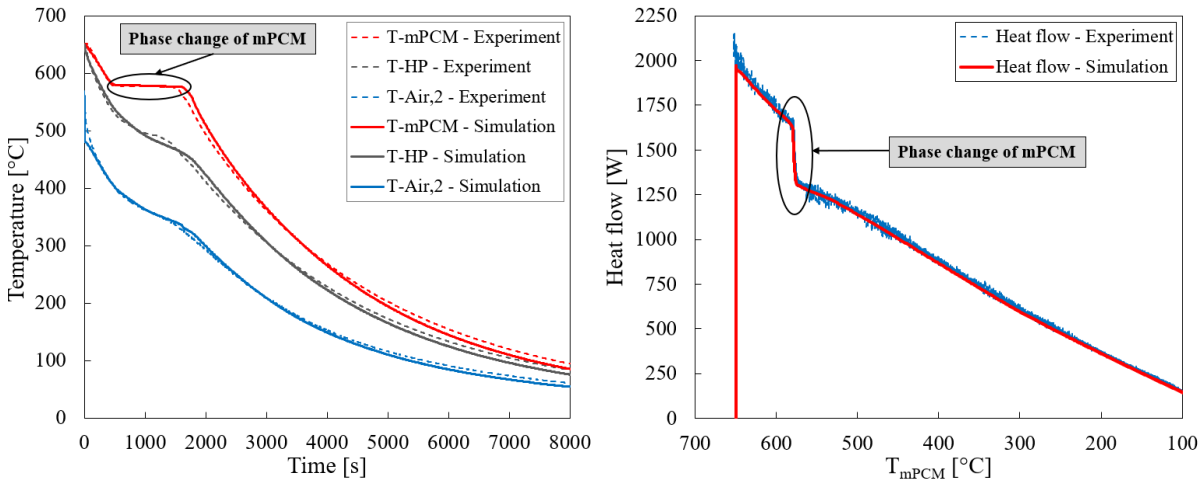

(a) Temperature versus discharge time **(b)** Heat flow versus mPCM temperature

Figure 3. Comparison of simulation results for temperature and heat flow with experimental data.

Table 2 gives the empirically determined values for the thermal contact resistance at the mPCM-graphite interface. The empirical analysis showed that the time for mPCM solidification and thermal discharge exhibit high sensitivity to the definition of thermal contact resistances. The thermal contact resistance at the interface is temperature dependent. It is at its lowest in the liquid state of the mPCM, increases sharply during the phase change and continues to rise gradually as the temperature decreases.

Table 2. Thermal contact resistances at mPCM-graphite interface based on empirical study.

Interface	Temperature range [°C]	Thermal contact resistance [cm^2K/W]
mPCM – Graphite	650 to 575	0.7
	575 to 525	12.5 to 37
	525 to 300	37 to 60
	300 to 100	60 to 70
	< 100	70

Figure 4 shows the liquid mass fraction as seen from a cross-section of the mPCM volume at various stages of its phase change from liquid to solid. The liquid mass fraction of the mPCM volume directly quantifies the amount of latent heat in the phase change material. A liquid fraction of 1 indicates fully liquid and a liquid fraction of 0 indicates fully solid. Regions where the liquid fraction is between 1 and 0 are called mushy zones. Figure 4(a) shows the initial start of the phase change at t = 291 s. Figure 4(b) illustrates that at t = 651 s, the liquid fraction starts to decrease first in the mPCM volume near to air inlet side, with the upper right regions that are further away from the air inlet being completely liquid. In figure 4(c) at t = 1011 s, the volume close to the air inlet begins to solidify completely, while large regions are still in the mushy zone. In figure 4(d) at t = 1771 s, the complete volume of the storage material is in the solid state. The solidification time for the volume average of liquid fraction from 1 to 0 in the simulation is 1480 s. It can be concluded that despite the high thermal conductivity of the storage material $AlSi_{12}$ and the relatively small overall dimensions of the prototype, there is a noticeable impact on the direction of solidification depending on the orientation of the air discharge flow.

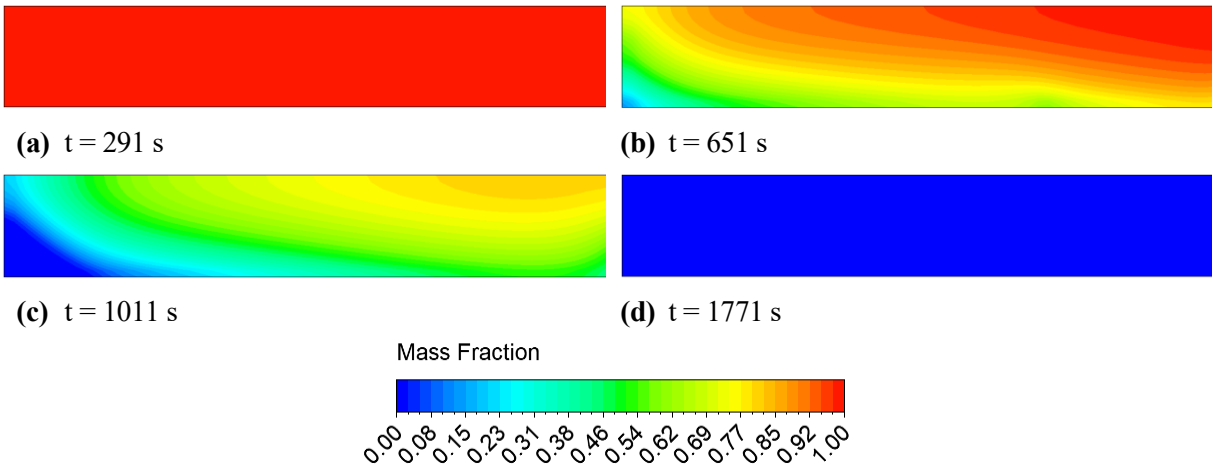

Figure 4. Liquid mass fraction of mPCM cross-section at various stages of solidification quantifying the discharge of latent heat.

Figure 5 gives the overall temperature distribution at a cross-sectional view of the fluid channel, mPCM, heating steel plate, graphite and steel container during the phase change at t = 1011 s. Based on the temperature contours, strong temperature gradients exist in the air fluid and solid parts. The air temperature gradually increases from inlet to outlet in x-direction, generating an unequal temperature distribution in flow direction in the adjacent parts and the mPCM. Consequently, the heat flux is higher at the channel inlet than at the outlet. The resulting temperature gradient in the mPCM is 6 K.

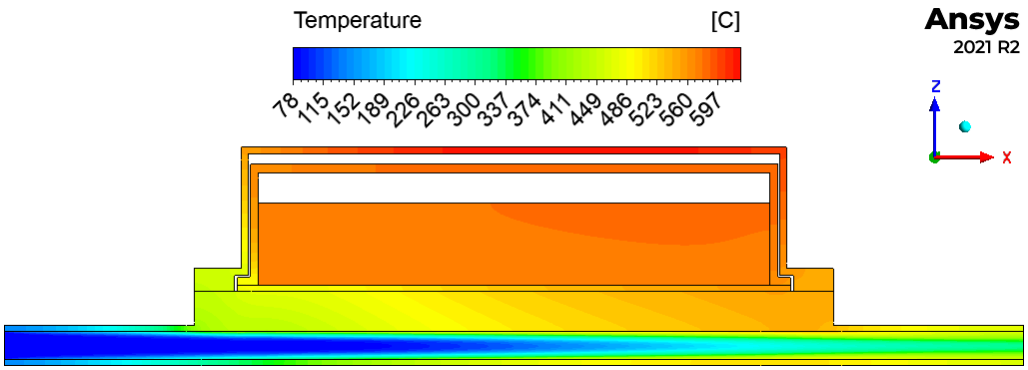

Figure 5. Temperature distribution at cross-section after t = 1011 s thermal discharge.

4. Conclusion

By means of a three-dimensional computational fluid dynamics model, the transient conjugate heat transfer of a novel metallic latent heat storage concept was simulated. For validation of the numerical model, the results of the simulations were compared to the available experimental data. The transient thermal discharge was simulated from 650 °C to 100 °C, and the solidification of the storage material at around 577 °C was simulated using an enthalpy-porosity approach. The discharge time and total heat flow showed good agreement with the experimental data, indicating the model's successful validation. An empirical study was carried out to determine the thermal contact resistance at the interface between the storage material and the graphite container. The transition from liquid to solid is associated with a significant rise in thermal contact resistance. Observation of the liquid fraction during the phase change showed that the storage material solidifies faster near to the air inlet due to high temperature gradients along the fluid flow direction. The present study contributes a validated numerical model and new physical insights regarding the thermal discharge of a metallic LHTES.

Acknowledgements

This work was supported by the WM-BW (Wirtschaftsministerium Baden-Württemberg) within the project ‘THS-Bus’ and the EFRE (Europäischer Fonds für regionale Entwicklung) Leitmarktwettbewerb Nordrhein-Westfalen Mobilität.Logisitk within the project ‘Lathe.Go’.

References

[1] Großmann H 2013 *Pkw-Klimatisierung: Physikalische Grundlagen und technische Umsetzung* (Berlin, Heidelberg: Springer)
[2] Zhang Z, Li W, Zhang C and Chen J 2017 *Applied Thermal Engineering* **110** 1183–8
[3] Jankowski N R and McCluskey F P 2014 *Applied Energy* **113** 1525–61
[4] Shamberger P J and Bruno N M 2020 *Applied Energy* **258** 113955
[5] Rawson A J, Kraft W, Gläsel T and Kargl F 2020 *Journal of Energy Storage* **32** 101927
[6] Kraft W, Stahl V and Vetter P 2020 *Energies* **13** 3023
[7] Luo C, Xie P, Chen G, Mao L, Liu L, Jin L, Cheng Z, Xu J and Qiao G 2022 *Journal of Energy Storage* **51** 104393
[8] Nees F, Katourtzidis A, Kraft W, Stahl V and Vetter P 2022 *Proc. 8th World Congress on Mechanical, Chemical, and Material Engineering (MCM'22)* (Prague, Czech Republic)
[9] Nees F, Feine J, Katourtzidis A, Stahl V and Kraft W 2023 *Proc. 17th Int. Heat Transfer Conf., IHTC-17* (Cape Town, South Africa)